
This is an electronic reprint of the original article.
This reprint may differ from the original in pagination and typographic detail.

Mughal, M. R.; Ali, H.; Ali, A.; Praks, J.; Reyneri, L. M.

Optimized Design and Thermal Analysis of Printed Magnetorquer for Attitude Control of Reconfigurable Nanosatellites

Published in:
IEEE Transactions on Aerospace and Electronic Systems

DOI:
[10.1109/TAES.2019.2933959](https://doi.org/10.1109/TAES.2019.2933959)

E-pub ahead of print: 01/01/2019

Document Version
Peer reviewed version

Please cite the original version:
Mughal, M. R., Ali, H., Ali, A., Praks, J., & Reyneri, L. M. (2019). Optimized Design and Thermal Analysis of Printed Magnetorquer for Attitude Control of Reconfigurable Nanosatellites. IEEE Transactions on Aerospace and Electronic Systems. <https://doi.org/10.1109/TAES.2019.2933959>

This material is protected by copyright and other intellectual property rights, and duplication or sale of all or part of any of the repository collections is not permitted, except that material may be duplicated by you for your research use or educational purposes in electronic or print form. You must obtain permission for any other use. Electronic or print copies may not be offered, whether for sale or otherwise to anyone who is not an authorised user.

Optimized Design and Thermal Analysis of Printed Magnetorquer for Attitude Control of Reconfigurable Nanosatellites

M. Rizwan Mughal^{1,2}, Hassan Ali³, Anwar Ali⁴, Jaan Praks¹, Leonardo M. Reyneri⁵

¹Department of Electronics and Nano engineering, School of Electrical Engineering, Aalto University, 02150, Espoo, Finland

²Department of Electrical Engineering, Institute of Space Technology, Islamabad, Pakistan

³Department of Space Science, Institute of Space Technology, Islamabad, Pakistan

⁴School of Information Science and Technology, Zhejiang Sci-Tech University, Hangzhou 310018, China

⁵Department of Electronics and Telecommunications, Politecnico di Torino, 10129, TO, Torino, Italy

Corresponding Author: rizwan920@gmail.com

Abstract— Attitude Control System (ACS) is one of the critical subsystems of any spacecraft and typically is in charge of de-tumbling, controlling and orienting the satellite after initial deployment and during the satellite operations. The magnetorquer is a core magnetic attitude control actuator and, therefore, a good choice for nanosatellite attitude stabilization. There are various methods to achieve control torque using the magnetorquer. An innovative design of printed magnetorquer has been proposed for the nanosatellites which is modular, scalable, cost effective, less prone to failure, with reduced harness and power consumption since the traces are printed either on top layer or inner layers of the printed circuit board. The analysis in terms of generated torque with a range of input applied voltages, trace widths, outer and inner-most trace lengths is presented to achieve the optimized design. The optimum operating voltage is selected to generate the desired torque while optimizing the torque to the power ratio. The results of analysis in terms of selection of optimized parameters including torque to power ratio, generated magnetic dipole moment and power consumption have been validated practically on a cubesat panel. The printed magnetorquer configuration is modular which is useful to achieve mission level stabilization requirements. For spin stabilized satellites, the rotation time analysis has been performed using the printed magnetorquer.

Keywords—*printed magnetorquer; attitude control; small satellites; thermal analysis; nanosatellites*

I. INTRODUCTION

Nanosatellites have gained great attention of the space community since last decade and have a key role in current and future space industry with potentially great impact [1]. The nanosatellites, being affordable, can be used in core application fields including remote sensing, earth observation, radiometry, interferometry to name a few [2], [3], [4]. The small size, mass, cost and low power features make them an obvious choice for universities and small and medium enterprises (SMEs). The Attitude Control System (ACS) controls and stabilizes the orientation of spacecraft after deployment from the launch vehicle and during its mission life. After separation from the launch vehicle, the spacecraft is mostly tumbling. It has to deal with large rotations and high angular rates in the early orbit life.

In order to control its orientation and to stabilize in the required direction (i.e. targeting the earth observational payload (camera) towards the earth and solar panels towards the sun and antennas towards the ground station), a number of sensors and actuators are required [5]. The attitude determination system determines the orientation of the satellite whereas the attitude control system performs the de-tumble and control maneuvers [6].

A block diagram representing attitude determination sensors and attitude control techniques is represented in Fig. 1. For remote sensing and earth observation applications, the attitude control maintains pointing with required pointing accuracy whereas for spin stabilized spacecrafts, it maintains the required spin rate along the desired rotational axis. The passive control systems including permanent magnets and gravity gradients are easy to develop with lower development costs and consume no power but they do not fulfill the controlled stabilization requirements of most of the missions [7]

In a permanent magnet passive attitude control system, a set of permanent magnets on board the satellite align the satellite with the magnetic field lines of the earth. The attitude of passive satellite is a

function of the orbit and the magnetic field lines along the orbit. Therefore the orbit inclination has huge impact on the pointing of the satellite. The spacecrafts like KeySat-1, QuakeSat, Delfi-C3, and GeneSat are few examples of passively stabilized with permanent magnets. The main advantages are simplicity, no power consumption and reliability of the system. The major drawbacks of the passive control is that one cannot use it for orientation control. Since modern day missions require a very fine pointing accuracy, therefore the passive control is not a suitable control system anymore.

Gravity gradient is another passive attitude stabilization technique which keeps one axis of the satellite aligned to earth's local vertical direction. It uses the change in gravity with altitude to create torque so one face of the satellite always faces in the downward direction. Typically, long booms are usually extended to create the torque. In [8], Kiaying Zhio discusses the magnetic attitude control for earth pointing satellites in the presence of gravity gradient. The main advantages of this scheme are simplicity, no power consumption and long lifetime. The drawbacks are poor pointing accuracy, tendency to flipping upside down, and potential of thermally bending of boom causing oscillations.

The active control systems (magnetic rods, gyroscopes, reaction wheels, momentum wheels, and spin control systems) are widely used in a three axes stabilized spacecraft for better pointing accuracy [9]. The main constraint in the active attitude control is the added hardware in a small available volume and generally requires 1/3rd of the total volume for a 3U CubeSat. This work analyzes the design solutions for light weight, low power consumption magnetic attitude control system using printed magnetorquer coils to optimize the design in terms of power, available area and generated torque. The principle of operation is based on the generation of magnetic field through a current carrying coil. The interaction of the generated magnetic dipole moment with that of the earth magnetic field results in control torques which are necessary for the attitude control of the satellite [5], [10]. Currently, there are very limited designs and developments in the printed magnetorquers for cubesat applications. In [11], [12] the authors present a tradeoff analysis of printing different shapes of embedded magnetorquers and provide the more feasible shapes keeping into consideration

the cubesat form factor. Niccolò Bellini present the design techniques for optimized air core and printed magnetorquers [13]. A commercially available CubeSat product also integrates the magnetorquer inside the PCB layers [14]. The designs presented in literature not fully optimized in terms of selection parameters. This work describes the development of reconfigurable printed magnetorquer with its performance comparison with the state of the art. The numerous advantages of the presented design approach over the traditional designs are presented in this paper. The optimized design provides flexibility in the selection of design parameters and can be utilized in any satellite configuration.

The implementation of the printed magnetorquer has been performed for AraMiS and Foresail satellites. The AraMiS architecture is based on panel based nanosatellites which simplifies the satellite design process and helps achieve modular, scalable and plug and play designs [15] [16] [17]. This architecture uses the symmetric panels arranged in payload specific configurations. A number of small, flexible and powerful modules are embedded on each panel. These modules are pre-tested, therefore the integration can be done much faster. These panels are quickly assembled in standard CubeSat structure as well as custom configurations [18][32][33]. The PCB of one such panel contains four layers of printed magnetorquers in addition to all necessary electronics as shown in Fig. 2. The Foresail satellites require spin stabilization along the axis to monitor the environmental interactions using particle telescope (PaTe) and to de orbit the spacecraft using electric plasma brake (EPB) [19], [20]. The spacecraft is currently under development and utilizes the printed magnetorquers in addition to the air core magnetorquers for attitude control.

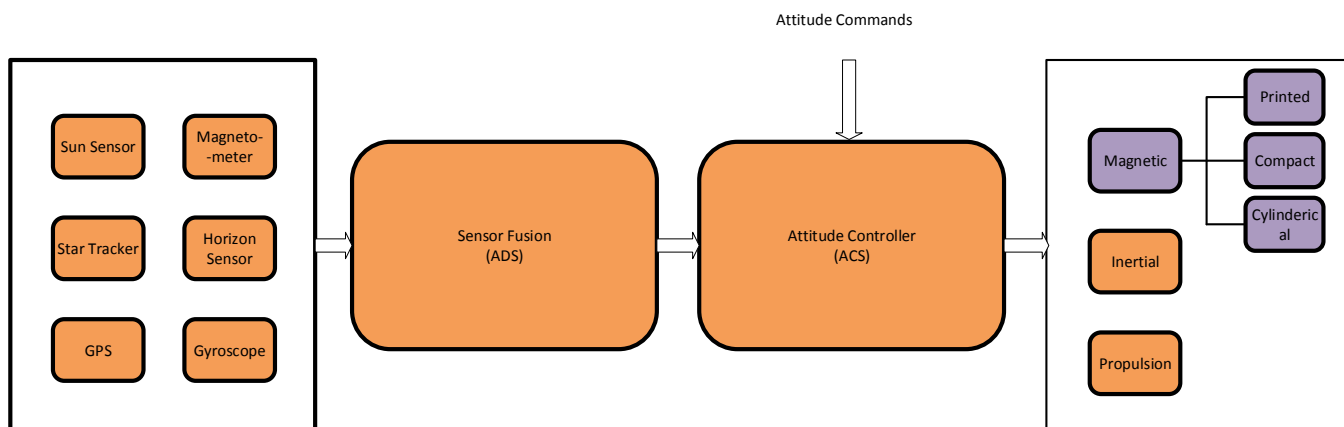


Fig. 1 A block level representation of attitude sensors and attitude actuators

The presented design can be printed on top or embedded in as many internal PCB layers as desired based on the required dipole moment. For the generation of magnetic moment, selected parameters are the inner and outer dimension of the printed coils (W_0 , W_I), trace widths and their separation based on PCB design rules. The design permits enough space for the placement of other discrete components on the printed layer and the placement strategy also overcomes the residual magnetic fields.

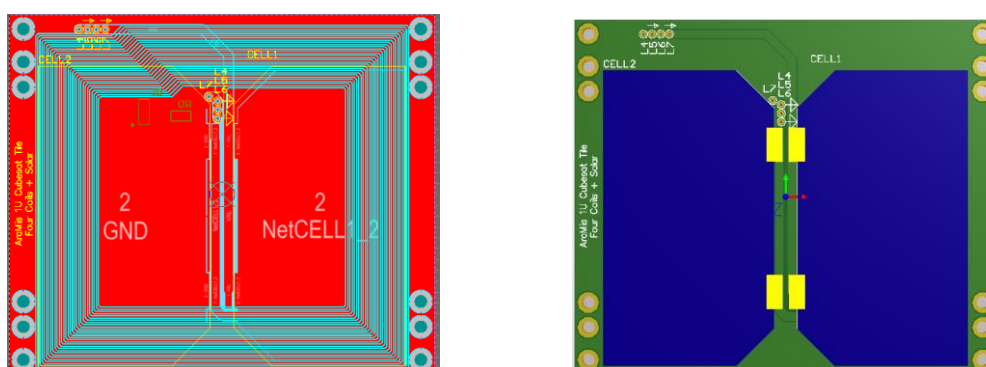


Fig. 2 A multilayered panel with printed magnetorquer

The simplified block diagram of the attitude determination and control system using printed magnetorquer is depicted in Fig. 3. For the current attitude estimation, raw sensor measurements are compared against the known models. The raw values of magnetometer and sun sensors are compared against the known reference models for estimation of the current attitude of the spacecraft. For magnetic field modeling, the International Geomagnetic Reference Field (IGRF) [9] is typically used; and for sun direction modeling, the method described in Montenbruck and Pfleger (1994) is used. Having the estimate of the current attitude, the controller issues torque commands for desired orientation [9], [21], [22]. The closed loop feedback ensures the maintenance of desired attitude control by repeating the torque command until the desired orientation is achieved [23], [24], [25], [26].

II. PRINTED MAGNETORQUER

The designed printed embedded magnetorquer is fully compliant with the cubesat dimensions and requires no extra space since the traces are either printed or embedded in the internal layers of the board as shown in Fig. 2. The design selection can be chosen among multiple reconfigurable options which are presented. The detailed analysis of printed coils in terms of selection of outer dimensions, inner dimensions and trace widths has been performed against key design parameters including the generated magnetic moments, the consequent torques, torque to the power ratios and expected temperature rise due to the flow of current through the panel.

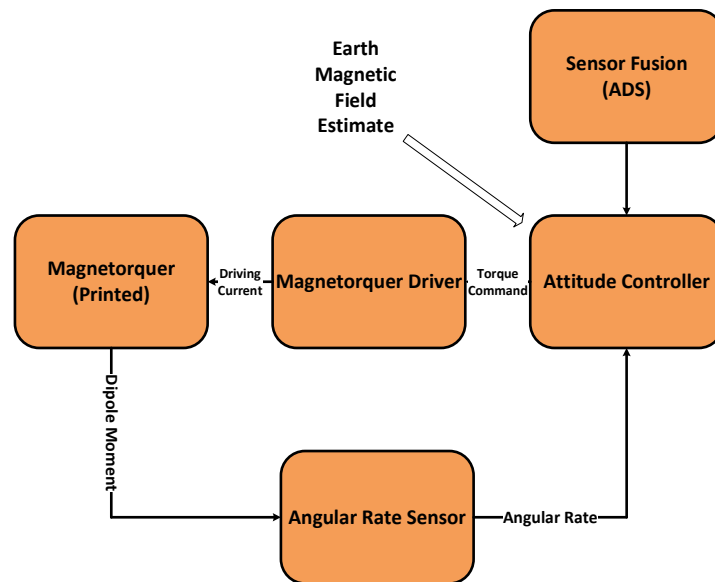


Fig. 3 Design flow of attitude control using printed magnetorquer

The main objective of this magnetorquer design is not only being light weight but also being able to generate required magnetic moment with the available power. The traces are printed in square shape for a 1U cubesat panels. The dimension of single coil is shown in Fig. 4 and Fig. 5 with key design parameters highlighted. The design can be printed in any configuration as highlighted in [17], [27].

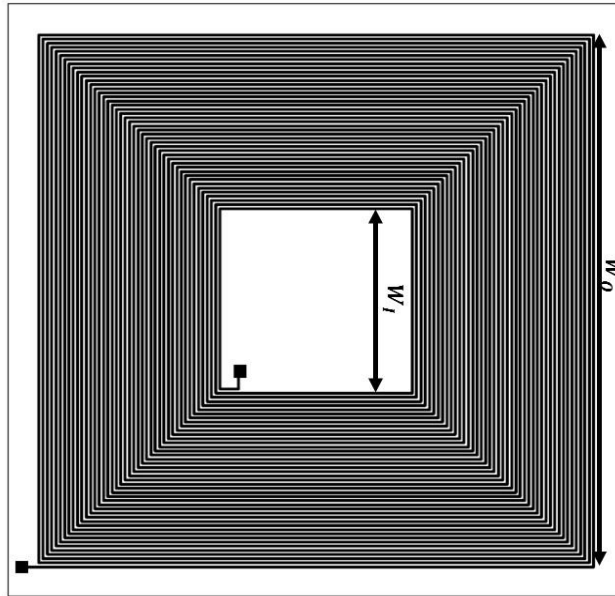


Fig. 4 Dimensions and cross-sectional view of printed magnetorquer

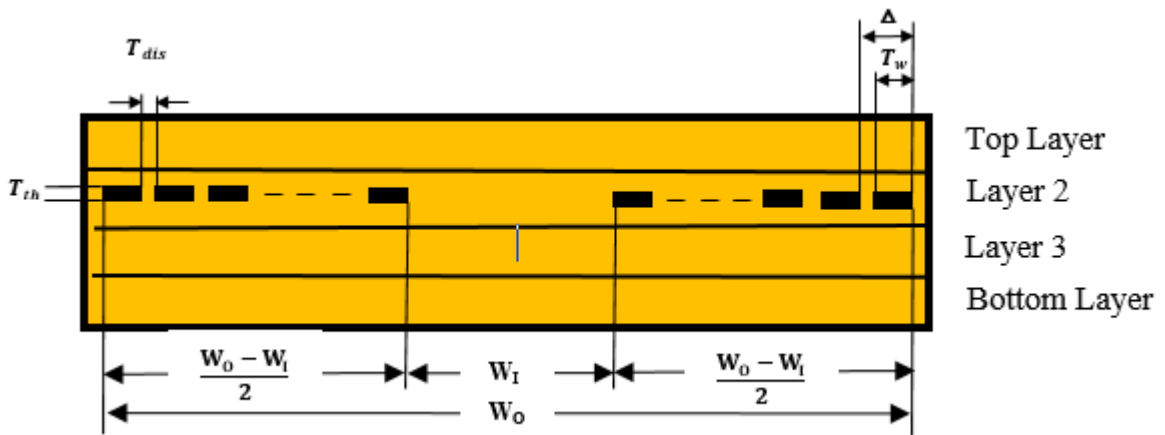


Fig. 5 Cross sectional view of printed magnetorquer

III. PRINTED MAGNETORQUER OPERATION AND ANALYSIS

The printed magnetorquer works on the principle of generation of magnetic moment by the flow of current through the coil, which interacts with the earth magnetic field and produces torque, used for the desired rotation. The magnetic moment (μ) is dependent on current (I) through the printed traces, the effective area of the printed coils (A) and the total number of turns (N). The area (A) encompassed by the printed configuration is dependent on several factors including the outer and inner dimensions of the printed magnetorquers (W_o and W_i respectively), size of panels, separation between traces (T_{dis}), trace widths (T_w) and cumulative trace width and separation ($\Delta = T_w + T_{dis}$). The printed magnetorquer as shown in Fig. 4 is printed in a cubesat panel. It has symmetric trace prints separated apart by Δ , therefore, the total length of each complete layer (L_t) of the printed magnetorquer can be approximated as sum of individual lengths of subsequent squares. Any square with trace i has length $L_i = 8\Delta \cdot i$, where 8Δ is the perimeter increase from trace i to $i+1$. The total length of complete layer, L_t , is given by

$$L_t = \sum_{i_{min}}^{i_{max}} 8\Delta \cdot i \quad (1)$$

The lengths of inner and outer squares changes between $i_{min} = \frac{W_i}{2\Delta}$ (i.e. perimeter $4W_i$) and $i_{max} = \frac{W_o}{2\Delta}$

(i.e. perimeter $4W_o$). For the sake of understanding, if we consider only three printed squares in a single panel, then the expression for L_t can be written as

$$L_t = 8\Delta \cdot i_{min} + 8\Delta(i_{min}+1) + 8\Delta \cdot i_{max}$$

The expression for total length L_t of Eq. (1) can be further generalized and is presented in following equations.

$$L_t = 8\Delta \left(\frac{(i_{\max})(i_{\max} + 1)}{2} - \frac{(i_{\min})(i_{\min} - 1)}{2} \right) \quad (2)$$

$$L_t \approx \frac{8\Delta(i_{\max}^2 - i_{\min}^2)}{2} \quad (3)$$

$$L_t = 4\Delta \left(\left(\frac{4W_0}{8\Delta} \right)^2 - \left(\frac{4W_1}{8\Delta} \right)^2 \right) \quad (4)$$

$$L_t = \frac{(W_0^2 - W_1^2)}{\Delta} \quad (5)$$

The above expression is used for the computation of total trace length of the printed magnetorquer for given inner and outer dimensions. Any printed square, i , in Fig.4 encompasses area W_i^2 , therefore the total area (A) of a single layer of printed magnetorquer can be computed as sum of areas of individual printed squares and is given in Eq.(6).

$$A = \sum_i (W_i)^2 = \sum_i (2\Delta i)^2 = 4\Delta^2 \sum_{i_{\min}}^{i_{\max}} i^2 \quad (6)$$

The total area of the magnetorquer depends on the shape of the printed traces. For the selected shape of Fig. 4, we can use (7) to compute the total area of the printed magnetorquer.

$$A = 4\Delta^2 \frac{(W_0)(W_0 + 2\Delta)^2 - (W_1)(W_1 + 2\Delta)^2}{24\Delta^3} \quad (7)$$

Assuming $\Delta \ll W_I, W_O$; the simplified expression is given by (8)

$$A \approx \frac{W_O^3 - W_I^3}{6\Delta} \quad (8)$$

The above equation provides useful selection criteria for the computation of total area of a single layer of the printed magnetorquer of Fig. 2 and Fig. 4. It is evident from (8) that; to maximize the magnetorquer area, the distance between the traces should be kept minimum allowable.

The design is optimized by analyzing the parameters including the torque (τ) and torque to power ratio (τ/P) by varying the applied voltage, trace width, inner and outer dimensions of the magnetorquer. The final design is selected based on the best achievable τ/P for the selected applied voltage. The maximum torque (τ) is exerted when the printed magnetorquer with a given magnetic moment is perpendicular to the magnetic field. The amount of generated torque is given by.

$$\tau = \mu \times B = |\mu||B| \quad (9)$$

Where μ is the magnetic dipole moment created by each magnetorquer and \mathbf{B} is the earth magnetic field vector. For the x,y,and z magnetorquers (expressed as spacecraft body fixed frame), the expression for the torque can be written as

$$\begin{pmatrix} \tau(x) \\ \tau(y) \\ \tau(z) \end{pmatrix} = \begin{pmatrix} 0 & B_z & -B_y \\ -B_z & 0 & B_x \\ B_y & -B_x & 0 \end{pmatrix} \begin{pmatrix} \mu(x) \\ \mu(y) \\ \mu(z) \end{pmatrix} \quad (10)$$

For the design optimization, we consider a single arbitrary reference axis in our future discussions to avoid computational complexity. We will consider the effective torques produced when magnetic field lines are normal to the reference axis in order to simplify the design calculations. The expression for torque, τ , for the printed magnetorquer is expressed in the following expressions.

$$\tau = \frac{(W_0^3 - W_I^3)}{6\Delta} \frac{V\Delta A_{\text{cross}}}{\delta(W_0^2 - W_I^2)} B \quad (11)$$

$$\tau = \frac{W_0 V B A_{\text{cross}} \left(1 - \left(\frac{W_I}{W_0}\right)^3\right)}{6\delta \left(1 - \left(\frac{W_I}{W_0}\right)^2\right)} \quad (12)$$

The power dissipation by the magnetorquer depends on the current consumed and the resistivity of copper traces (δ) which can be computed by (13).

$$P = \frac{V^2}{R} = \frac{V^2 \Delta A_{\text{cross}}}{\delta(W_0^2 - W_I^2)} \quad (13)$$

$$\text{Where } R = \frac{\delta L_t}{A_{\text{cross}}} = \frac{\delta(W_0^2 - W_I^2)}{\Delta A_{\text{cross}}} \quad (14)$$

The resistivity of the copper traces is directly proportional to the length of traces and inversely proportional to the cross-sectional area. The cross-sectional area depends upon the trace width and trace thickness ($A_{\text{cross}} = T_w \times T_{\text{th}}$). Now, given the expressions for power (P) and torques (τ) in Eqs. (12) and (13), we can compute τ/P for our design which is given by (15).

$$\frac{\tau}{P} = \frac{B(W_0^3 - W_I^3)}{6(T_w + T_{dis})} \left(\frac{1}{V}\right) \quad (15)$$

The above expression suggests that the torque to power ratio (τ/P) is inversely proportional to the applied input voltage. This ratio decreases by increasing the applied voltage (V), trace widths and their separation. The relationship of τ/P with the total length of the embedded coils is given by (16) and (17).

$$\frac{\tau}{P} = \frac{W_0 B A_{cross} \left(1 - \left(\frac{W_I}{W_0}\right)^3\right) \delta L_t}{V 6 \delta \left(1 - \left(\frac{W_I}{W_0}\right)^2\right) A_{cross}} \quad (16)$$

$$\frac{\tau}{P} = \frac{W_0 B \left(1 - \left(\frac{W_I}{W_0}\right)^3\right)}{V 6 \left(1 - \left(\frac{W_I}{W_0}\right)^2\right)} L_t \quad (17)$$

It can be concluded from (17) that the τ/P increases as the length of the coil (L_t) increases. As a consequence to this, the area and number of traces also increases resulting in manifold increase in τ/P . Since trace width and trace thickness are key design selection parameters in the printed magnetorquers, their dependency on τ/P is given by (18).

$$\frac{\tau}{P} = \frac{B(W_0^3 - W_I^3)}{6V\Delta} \quad (18)$$

The trace thickness has a constant effect since it is fixed dependent on the manufacturing of the board and the trace width has an inverse proportionality relation on the τ/P for the printed design provided other variables are kept constant.

Since the shape of the printed magnetorquer is not uniform, therefore the resultant force and exerted torque due to each segment is not uniform. Since each square is shorter than the previous one by a factor Δ ; therefore the net resultant force is the summation of all individual forces. The resultant force is maximum when the direction of current carrying trace is perpendicular to the external magnetic field. The resultant Lorentz force due to each sub-segment can be computed by placing the current carrying printed coil in magnetic field plane **B**. The strength of each part of the coil parallel to the plane gives a contribution that can be generalized as proved by [13] and given in (19)

$$F_1 = 3 \Delta I \sin(90 + \theta) \quad (19)$$

The strength of each part of the coil perpendicular to the plane **B** gives a contribution that can be generalized as given in (20).

$$F_2 = n I \Delta B \quad (20)$$

Where n is the total number of subsequent squares in the design. The direction of these forces can be interpreted by use of Flemings Right Hand Rule [28] and the net force can be computed if magnitude and direction of the field vector is known.

IV. OPTIMIZATION ANALYSIS AND RESULTS

For the design optimization and analysis, we have plotted the generated torque τ , τ/P , power consumption and current flow against variations in trace widths for our printed magnetorquer as shown in Fig. 6. It is evident from the graphs that by increasing the trace width, the τ/P decreases for any selected applied voltage. Since the amount of generated torque increases with the increase in trace width, the power consumption also increases in large proportions therefore; decreasing the overall τ/P . The analysis has been performed for two

selected voltages (3.3V and 5V). As the selected trace width increases, there is significant increase in the torque but at the expense of consumed power and heat dissipation, which causes an upper limit on selection of τ/P . The design can be optimized by changing the trace width and obtaining the highest percentage rise in τ/P at a particular voltage.

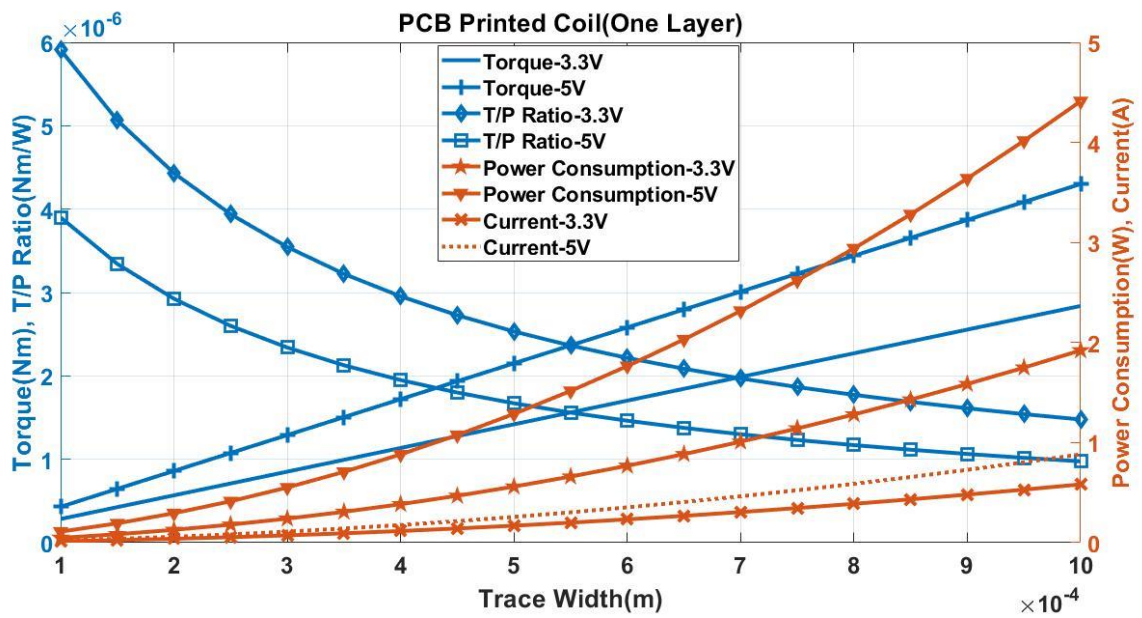


Fig. 6 Plot of trace width against torque, τ/P , Power and current

The selection of outer most and innermost dimensions as specified in Fig. 4 is another key design parameter. The analysis has been performed by changing the ratio of inner and outer dimensions of the printed traces (W_i/W_o). The resultant torque and torque to power ratio for two operating voltages (3.3V and 5V) is plotted in Fig. 7. As the magnetorquer encompasses more area of the printed circuit board, the generated torque and torque to power ratio increases. The total length of coil also increases by increasing the outer dimensions which causes the resistance to increase effectively permitting less current to flow in the magnetorquer. It can be concluded from the graph that for a fixed inner dimension, if the outer dimension increases, there is an

increase in torque to power ratio. As a design rule, the outer dimension should be larger in magnetorquer, if permitted by the board.

For fixed outer dimension, increasing the inner dimension causes a decrease in encompassed area of the magnetorquer, therefore limiting the number of traces. As a design rule, the smaller inner dimension generates more torque to power ratio which is better design selection.

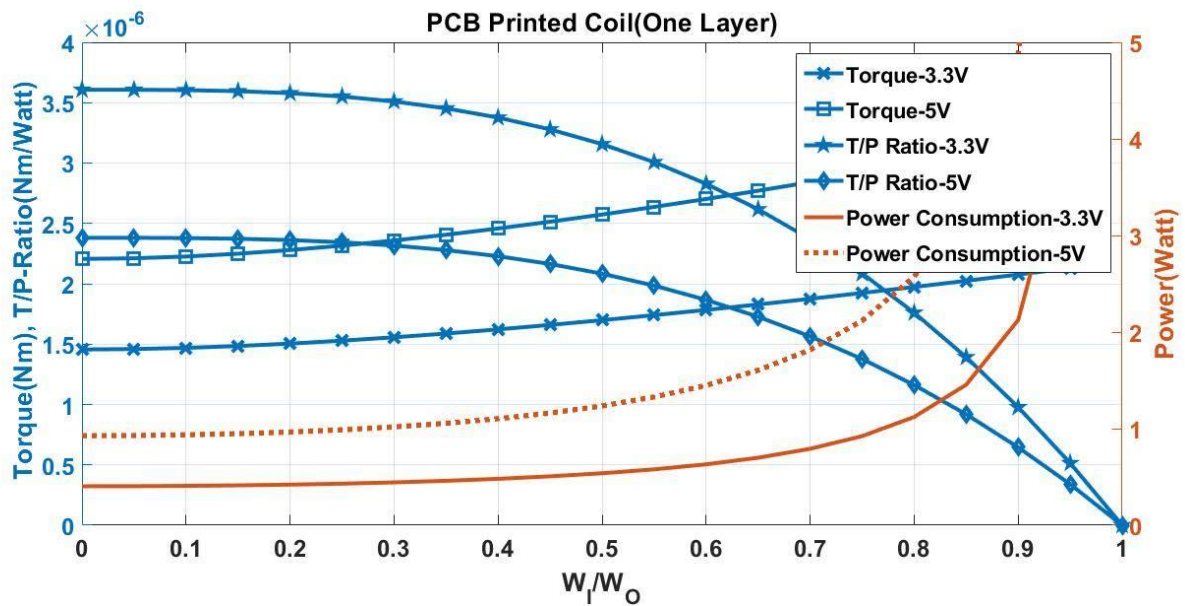


Fig. 7 Plot of W_1/W_0 against torque, τ/P and power consumption

The relation between torque, torque to power ratio (τ/P), power, current consumed by the coil against the applied voltage at selected trace widths is shown in Fig. 8. The torque and power consumption increases by increasing the applied voltages. According to (18), by increasing the applied voltage, there is rapid decrease

in τ/P . Therefore, we conclude that the lower applied voltage is more suitable for the design of printed magnetorquer since it provides more torque to power ratio.

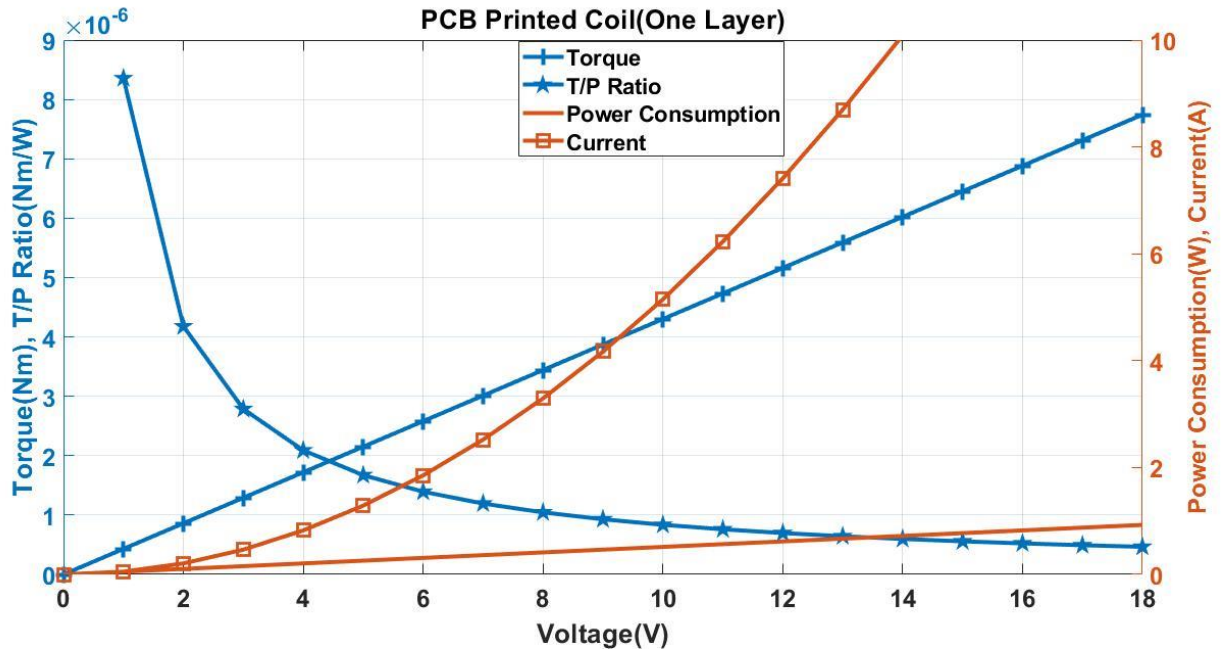


Fig. 8 Plot of operating voltage against torque, τ/P , power and current

The placement guidelines of multilayered magnetorquer in a single unit board were performed after optimization analysis. The optimized design parameters for a single layer are tabulated in Table 1. The design can be printed in a variety of configuration based on guidelines given in [17] and [27].

Table 1 Design parameters (single layer of printed magnetorquer)

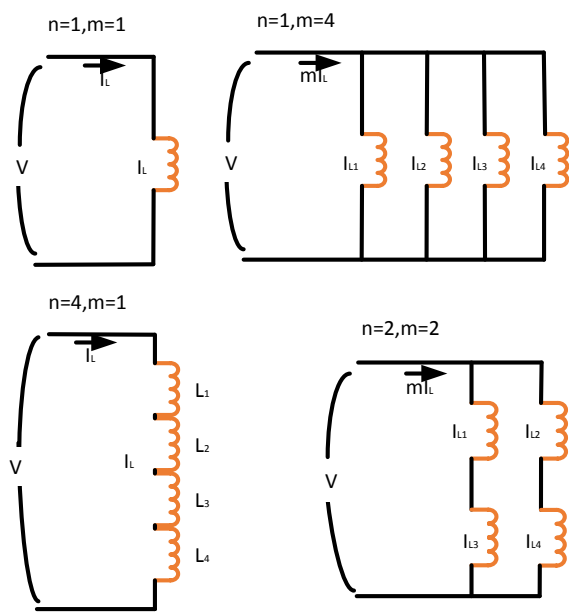
Parameter	Values
Average perimeter of coil	240 mm
Total length of single coil: L_t	10,285 mm
Outer dimensions: W_0	90mm

Inner dimensions: W_l	30mm
Trace thickness: T_{th}	18 μm
Trace width: T_w	0.5 mm
Cross sectional area: A_{cross}	$9 \times 10^{-9} \text{ m}^2$
Area of single layer: A	0.1671 m^2
Trace distance: T_{dis}	0.2 mm
Coil resistance: R	19.4 Ω
Copper resistivity: δ	$1.7 \times 10^{-8} \Omega \cdot \text{m}$
Generated dipole moment: μ	0.0284 Am^2
Operating voltage: V	3.3V

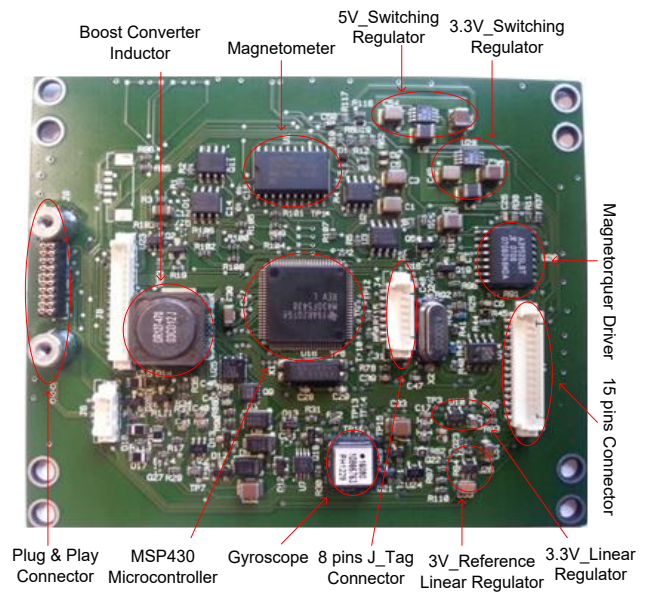
The modular magnetorquer can generate a range of magnetic dipole moments making the design quite flexible. The multilayered printed magnetorquers can be connected in different configurations (single, n in series, m in parallel and $n \times m$ in hybrid) to either maximize τ , minimize P or optimize τ/P [34]. In case of m parallel connected coils, the applied voltage is the same as that of a single coil (V) while the current drawn is mI_L as shown in Fig. 9(a). For n series connected coils; for the same applied voltage V , the flow of current is same as that of passing through a single coil (I_L). This configuration produces the same magnetic moment as generated by the single coil but consumes less power. In case of $n \times m$ hybrid combination, for the same applied voltage V , the current drawn by the magnetorquer is mI_L . The suggested reconfigurable options generate variable magnetic dipole moments and any of these configurations can be configured very quickly based on the mission pointing requirements. The parallel combination of m connected coils gives the maximum torque while consuming much more power. The series connected m coils optimize the available power while generating the same torque as that of a single coil.

The reconfigurable printed magnetorquers was realized on a multilayered panel of AraMiS satellites which is shown in Fig. 9(b). It consist of an eight layered printed board with internal four layers of reconfigurable

printed magnetorquer. The printed magnetorquer in each layer is reconfigurable and different combinations of the magnetorquers can be connected on top layer. The design parameters as used in Table 1 have been used in the AraMiS multilayered panel. The board also consist of a coil driver circuitry to deliver fixed applied voltage and variable current to the coils connected in any of the presented configurations. The integration of multilayered panel on a single unit cubesat is shown in Fig. 9(c). The detailed analysis of achievable torque to power ratio of the designed magnetorquer is presented in Table 2.



(a)



(b)



(c)

**Fig. 9 (a) Reconfigurable printed magnetorquers (b) Multi-layered panel with printed magnetorquer in internal layers
(c) Integration of multilayered panels in 1U cubeSat.**

The rotation and thermal analysis using the designed printed magnetorquer were performed for the spacecraft. The subsequent sections provide the rotation and thermal analysis of the single layered printed magnetorquers.

V. ROTATION TIME ANALYSIS

Given a satellite of known mass and moment of inertia along the spin axis, we can compute angular velocity achievable for a spinning spacecraft at a given applied voltage. The estcube and Foresail missions require a high spin rate along major axis of inertia while maintaining the sun pointing [29], [30]. The rotation time analysis was performed for a 1U cube using optimized magnetorquers. The analysis was performed to validate the printed magnetorquer for single axis attitude maneuvers. For the selected optimized magnetorquer parameters, the rotation time analysis was performed. The angular rotation acceleration (α) of the satellite

depends upon the applied torque (τ) and the moment inertia of the satellite (I_J) along the major rotational axis.

The moment inertia (I_J) along arbitrary major axis (taking Z axis) is given by:

$$I_{J_z} = \iiint_{-l_x/2}^{l_x/2} \rho(x^2 + y^2) dx dy dz \quad (21)$$

Where x, y, z are the Spacecraft Body Fixed Reference Frames (SBRF) and l_x, l_y and l_z are the respective lengths from the axis of inertia. After performing the integration function, the expression can be written as given in (22) and (23).

$$I_{J_z} = \left[\rho l_x l_y \frac{1}{12} (l_x^2 + l_y^2) z \right]_{z=-l_z/2}^{z=l_z/2} \quad (22)$$

$$I_{J_z} = \rho l_x l_y l_z \frac{1}{12} (l_x^2 + l_y^2) \quad (23)$$

Now since mass is a function of ($m = \rho l_x l_y l_z$); therefore

$$I_{J_z} = m \frac{1}{12} (l_x^2 + l_y^2) \quad (24)$$

The relationship between angular acceleration (α) and torque as given by (25).

$$\tau = I_J \alpha \quad (25)$$

The angular displacement (φ) is given by (26) [24].

$$\varphi = \alpha \left(\frac{t_\varphi}{2} \right)^2 \quad (26)$$

Where t_φ is the time taken to rotate the spacecraft axis by desired angle φ . Combining equation (25) and (26), we get:

$$t_\varphi = \left(\frac{2I_J \varphi}{\tau} \right)^{\frac{1}{2}} \quad (27)$$

In order to compute the torque required for the desired rotation, we use (28).

$$\tau = \frac{2 \cdot I_J \varphi}{t_\varphi^2} \quad (28)$$

For a spin stabilized spacecraft, this expression is useful to calculate the torque required to spin an initially stationary axis of the spacecraft by a certain angle. In order to rotate the spacecraft at a particular rotation rate, an added torque is required for longer time to achieve particular spin rate.

The generated magnetic moment was practically measured for all magnetorquer configurations of Fig.9(a). Based on the measurement results, the time taken to complete one revolution for a single unit cube was computed theoretically and compared with state of the art [13], [14]. The resultant τ/P was also computed for each configuration. It is evident from Table 2 that the achieved τ/P using any configuration of the designed magnetorquer is higher than that achieved using state of the art and commercial options.

For designed multilayered panel, different reconfigurable options were plotted as shown in Fig. 10. It can be concluded that for the same applied voltage the time taken by a single magnetorquer and four in series is the same but the series combination consumes less power as compared to the single coil. The parallel connected coils rotate the spacecraft four times faster but at the expense of power consumption.

Table 2 Rotation time analysis results for 1U CubeSat (3.3V)

Configuration		μ (Am²)	τ (μNm)	P (W)	Rotation time (s)	τ/P (μNm/W)
Commercial/ Reference designs (1U panel)	Gomspace Nanopower P110 [14]	0.038	1.90	3.3	119.67	0.57
	Ref [13] design (best case)	0.108	5.4	0.994	70.98	5.4
Multilayered Panel (1U panel)	Single coil (1 x 1)	0.0284	1.42	0.56	138.45	2.53
	4 coils in series (4 x 1)	0.0284	1.42	0.14	138.45	10.14
	4 coils in parallel (1 x 4)	0.4542	22.71	2.24	34.61	10.14
	Hybrid (2 x 2)	0.1136	5.68	0.56	69.22	10.14

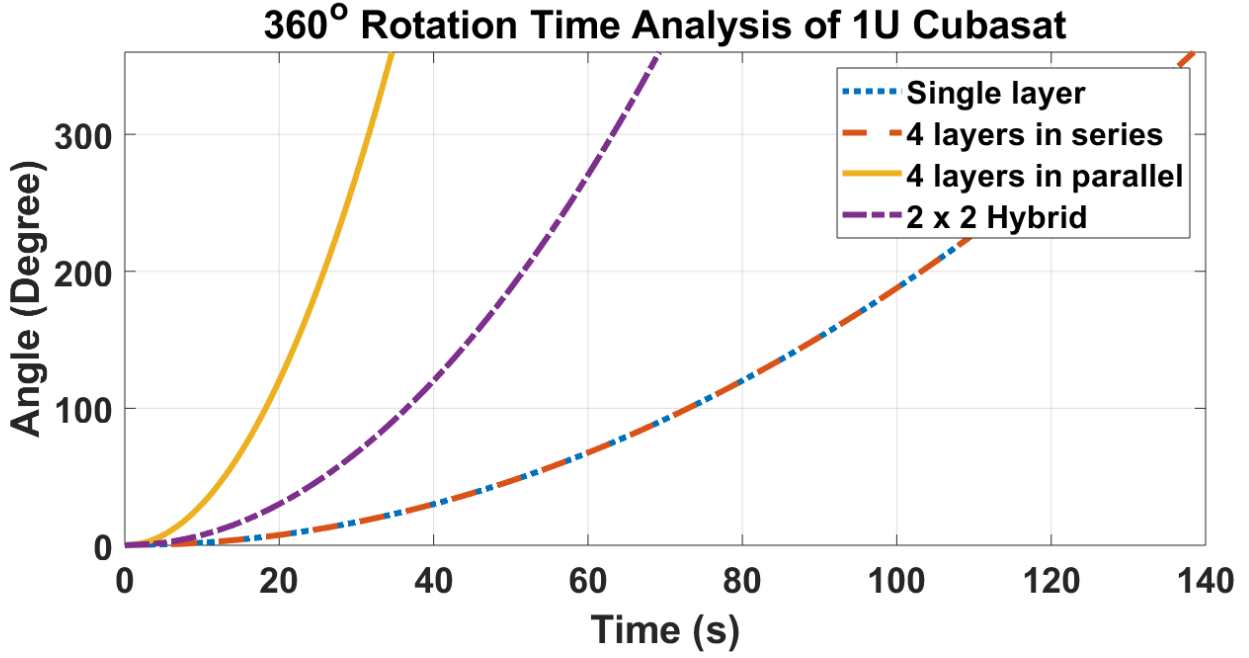


Fig. 10 Plot of rotation time against angular velocity using printed magnetorquer

VI. THERMAL ANALYSIS

The thermal balance analysis was performed to validate our design of magnetorquer. Since the printed coils may consume much power, therefore they are prone to heat dissipation. For a stable system, the heat balance equation is used which relates effective temperature due to the external environment T_{external} and temperature rise due to internal heat dissipating elements including magnetorquers, T_{internal} . The total thermal heat due to external environment, T_{external} , experienced by the CubeSat is given by (29).

$$T_{\text{external}}^4 = \frac{q_s}{\sigma} \left(\frac{1}{4} + F\alpha \right) + FT_E^4 \quad (29)$$

The radiation heat transfer is governed by Stefan-Boltzmann's Law [31], given by (30).

$$T_{\text{internal}}^4 = \frac{P}{\sigma \epsilon A} \quad (30)$$

The overall temperature for the cubesat can be computed by (29) and (30).

$$T^4 = T_{\text{external}}^4 + T_{\text{internal}}^4 \quad (31)$$

$$T = \sqrt[4]{\frac{q_s}{\sigma} \left(\frac{1}{4} + F\alpha \right) + FT_E^4 + \frac{P}{\sigma \epsilon A}} \quad (32)$$

Where $q_s = 1371 \text{ W/m}^2$, $\sigma = 5.67 \times 10^{-8} \text{ W/m}^2\text{K}^4$, $F = 0.15$, and $T_E = 255 \text{ K}$

The analysis computes the temperature rise due to the printed magnetorquers while neglecting all the other internal heat dissipations. The change in temperature of the CubeSat by varying the trace width of the printed magnetorquers is represented in Fig. 11 which signifies the direct dependence of temperature on power consumption and current passing through the coil. For the range of selected trace widths of the printed magnetorquer, the thermal analysis suggests that the increase in the trace widths have an exponential dependence on the temperature rise. Even if the temperature profile is exponential, the overall effect of increasing the trace widths of the printed magnetorquer for the worst case (4 coils in parallel) doesn't cause thermal imbalance issues.

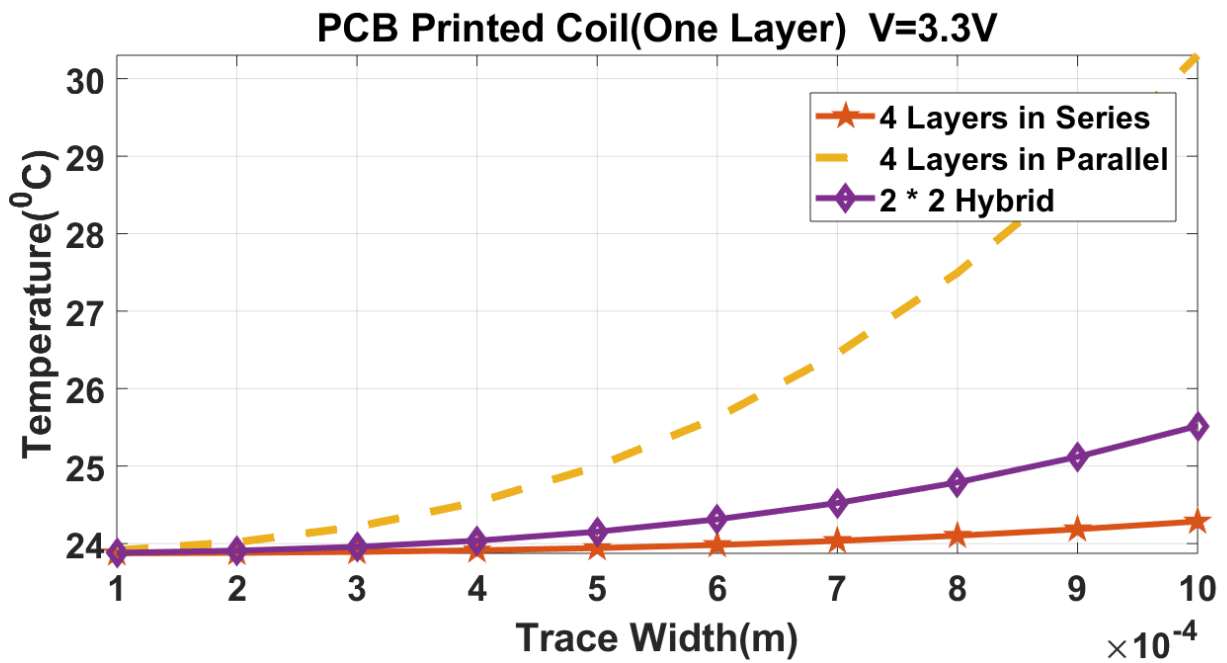


Fig. 11 Thermal effect by changing the trace width of printed magnetorquer

Fig. 12 shows the effect of variation in applied voltage against the temperature change for selected configurations of printed magnetorquers. It can be noticed from the figure that the overall temperature of cubesat increases exponentially at higher operating voltages but remains well within operational limits even for worst case of four coils in parallel. Therefore as a design selection, the lower operating voltages for the magnetorquer maintain better thermal balance.

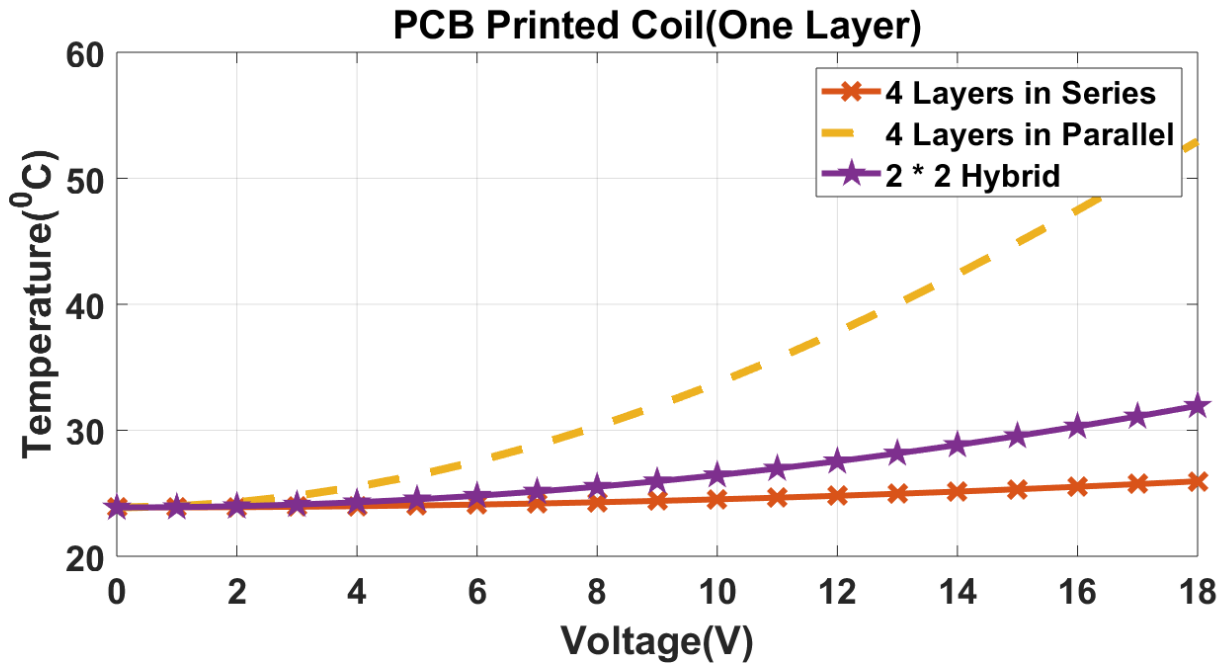


Fig. 12 Applied voltage against temperature rise for printed magnetorquers

VII. CONCLUSION

The paper has presented a design approach on printing the magnetorquer onto the panels of the CubeSat in order to reduce the harness mass and power consumption while achieving the desired magnetic dipole moment. The detailed analysis of printed magnetorquer in terms of generated magnetic moment, torques, torque to power ratio was presented against key design selections including applied voltage, trace widths, trace thickness and power consumption. A reconfigurable design of printed magnetorquer was presented to generate optimum torque and torque to power ratio. The reconfigurable design parameters were compared against the commercially available embedded magnetorquer. The thermal analysis on the selected configurations suggested the temperature increase within allowable limits therefore validating the design selections. The analysis of angular velocity along rotational axis for a spinning spacecraft was presented using the optimized designs. In future, we will validate the design for higher form factor satellite platforms.

VIII. REFERENCES

- [1] M. N. Sweeting, "Modern Small Satellites-Changing the Economics of Space," *Proceedings of the IEEE*, vol. 106, (3), pp. 343-361, 2018.
- [2] C. K. Pang et al, "Nano-satellite swarm for SAR applications: design and robust scheduling," *IEEE Transactions on Aerospace and Electronic Systems*, vol. 51, (2), pp. 853-865, 2015.
- [3] H. Carreno-Luengo et al., "3Cat-2—An Experimental Nanosatellite for GNSS-R Earth Observation: Mission Concept and Analysis," in *IEEE Journal of Selected Topics in Applied Earth Observations and Remote Sensing*, vol.9, no. 10, pp. 4540-4551, Oct. 2016.
doi: 10.1109/JSTARS.2016.2574717.
- [4] WJ, Blackwell, Braun, S, Bennartz, R, et al. An overview of the TROPICS NASA Earth Venture Mission. *Q J R Meteorol Soc.* 2018; 144 (Suppl. 1): 16– 26. <https://doi.org/10.1002/qj.3290>
- [5] Junquan Li, Mark Post, Thomas Wright, and Regina Lee, "Design of Attitude Control Systems for CubeSat-Class Nanosatellite," *Journal of Control Science and Engineering*, vol. 2013, Article ID 657182, 15 pages, 2013. <https://doi.org/10.1155/2013/657182>
- [6] R. Rocha and L. Rodrigues, "Photovoltaic panels as attitude sensors for artificial satellites," *IEEE Aerospace and Electronic Systems Magazine*, vol. 31, (11), pp. 14-23, 2016.
- [7] Marcela I. Martinelli, Ricardo S. Sánchez Peña, "Passive 3 axis attitude control of MSU-1 pico-satellite", *Acta Astronautica*, Volume 56, Issue 5, 2005, Pages 507-517, ISSN 0094-5765, <https://doi.org/10.1016/j.actaastro.2004.10.007>.
- [8] K. Zhou et al, "Magnetic attitude control for Earth-pointing satellites in the presence of gravity gradient," *Aerospace Science and Technology*, vol. 60, pp. 115-123, 01/01, 2017
- [9] Finlay, C. C., et al. "International geomagnetic reference field: The eleventh generation." *Geophys. J. Int.* 183(3), 1216 – 1230, 2010
- [10]] Y. W. Jan and J. C. Chiou, "Attitude control system for ROCSAT-3 microsatellite: a conceptual design," *Acta Astronaut.*, vol. 56, (4), pp. 439-452, 02/01, 2005. 5.

- [11] Z. Mukhtar, A. Ali, M. R. Mughal and L. M. Reyneri, "Design and comparison of different shapes Embedded Magnetorquers for CubeSat Standard Nanosatellites," 2016 International Conference on Computing, Electronic and Electrical Engineering (ICE Cube), Quetta, 2016, pp. 175-180. doi: 10.1109/ICECUBE.2016.7495218.
- [12] Anwar Ali, Zeeshan Mukhtar, Khalil Ullah, Leonardo Reyneri, "Design and comparison of embedded air coils for small satellites", Turk. J. Elec. Eng. & Comp. Sci., (2018), pages 1027 – 1040, doi:10.3906/elk-1701-112.
- [13] Niccolò Bellini, "Magnetic Actuators for Nanosatellite Attitude Control." , UNIVERSITA' DI BOLOGNA, 2014.
- [14] Nano power P110 datasheet, "High efficient solar panel for nano-satellite with integrated coarse sun sensor, magnetorquer and thermistor.", Gomspace document #1014192, 22 October 2018. Online: https://gomspace.com/UserFiles/Subsystems/datasheet/gs-ds-nanopower-p110-210.pdf?fbclid=IwAR3MLIVcUGdXfYOAUZxutCBm_Tk-K5vX90tNPKOlifednSoa1OoKFNHM96s
- [15] M. R. Mughal, A. Ali and L. M. Reyneri, "Plug-and-play design approach to smart harness for modular small satellites," Acta Astronaut., vol. 94, (2), pp. 754-764, 02/01, 2014.
- [16] M. Mughal, "Student research highlight smart panel bodies for modular small satellites," IEEE Aerospace and Electronic Systems Magazine, vol. 29, (12), pp. 38-41, 2014.
- [17] A. Ali et al, "Innovative power management, attitude determination and control tile for CubeSat standard NanoSatellites," Acta Astronaut., vol. 96, pp. 116-127, 03/01, 2014.
- [18] Elahi, H., Butt, Z., Eugnei, M. et al., "Effects of variable resistance on smart structures of cubic reconnaissance satellites in various thermal and frequency shocking conditions, J Mech Sci Technol (2017) 31: 4151. <https://doi.org/10.1007/s12206-017-0811-z>
- [19] Pekka Janhunen, "Electrostatic Plasma Brake for Deorbiting a Satellite", Journal of Propulsion and Power 2010 26:2, 370-372.
- [20] Osama Khurshid, Jorma Selkäinaho, Halil Ersin Soken, Esa Kallio, Arto Visala, "Small satellite attitude determination during plasma brake deorbiting experiment", Acta Astronautica, Volume 129, 2016, Pages 52-58, ISSN 0094-5765, <https://doi.org/10.1016/j.actaastro.2016.08.035>.
- [21] A. Slavinskis, H. Ehrpais, H. Kuuste, I. Sünter, J. Viru, J. Kütt, E. Kulu and M. Noorma, "Flight Results of ESTCube-1 Attitude Determination System," J. Aerosp. Eng., vol. 29(1):04015014.

- [22] Mohammed A. Desouky, Kaushik Prabhu, and Ossama O. Abdelkhalik. "On Spacecraft Magnetic Attitude Control", 2018 Space Flight Mechanics Meeting, AIAA SciTech Forum, (AIAA 2018-0205), <https://doi.org/10.2514/6.2018-0205>
- [23] L. Sahar et al, "Hard Disk Drive Based Reaction Wheels for CubeSat Attitude Control," *J. Spacecraft Rockets*, vol. 55, (1), pp. 236-241, 01/01; 2018/07, 2018.
- [24] M. Noman, S. M. Zulqamain, M. R. Mughal, A. Ali and L. M. Reyneri, "Component selection for magnetic attitude subsystem of PNSS-1 small satellite," 2017 8th International Conference on Recent Advances in Space Technologies (RAST), Istanbul, 2017, pp. 361-367. doi: 10.1109/RAST.2017.8002959
- [25] Y. Li, D. Ye and Z. Sun, "Robust finite time control algorithm for satellite attitude control," *Aerospace Science and Technology*, vol. 68, pp. 46-57, 09/01, 2017.
- [26] M. D. Pham et al, "Gain-scheduled extended kalman filter for nanosatellite attitude determination system," *IEEE Transactions on Aerospace and Electronic Systems*, vol. 51, (2), pp. 1017-1028, 2015.
- [27] Bradley Scott Cotten, "Design, Analysis, Implementation and Testing of the Thermal Control, and Attitude Determination and Control Systems for the Canx-7 Nanosatellite Mission." , University of Toronto, 2014.
- [28] Edward Hughes, John Hiley, Ian McKenzie-Smith, Keith Brown, *Hughes Electrical & Electronic Technology*. (12th ed.), 2016, ISBN 9781292093048, Pearson Education Limited, .
- [29] A. Slavinskis et al, "High spin rate magnetic controller for nanosatellites," *Acta Astronaut.*, vol. 95, pp. 218-226, 02/01, 2014.
- [30] B. A. Riwanto et al, "Particle Swarm Optimization With Rotation Axis Fitting for Magnetometer Calibration," *IEEE Transactions on Aerospace and Electronic Systems*, vol. 53, (2), pp. 1009-1022, 2017.
- [31] Boltzmann, L. (1884), Ableitung des Stefan'schen Gesetzes, betreffend die Abhängigkeit der Wärmestrahlung von der Temperatur aus der electromagnetischen Lichttheorie. *Ann. Phys.*, 258: 291-294. doi:10.1002/andp.18842580616
- [32] Boschetto, A., Bottini, L., Eugeni, M., Cardini, V., Nisi, G. G., Veniali, F., & Gaudenzi, P. (2019). Selective Laser Melting of a 1U CubeSat structure. *Design for Additive Manufacturing and assembly. Acta Astronautica*.
- [33] Elahi, H., Eugeni, M., Gaudenzi, P., Gul, M., & Swati, R. F. (2019). Piezoelectric thermo electromechanical energy harvester for reconnaissance satellite structure. *Microsystem Technologies*, 25(2), 665-672.

[34] A. Ali, M. R. Mughal, H. Ali, L. M. Reyneri and M. N. Aman, "Design, implementation, and thermal modeling of embedded reconfigurable magnetorquer system for nanosatellites," in IEEE Transactions on Aerospace and Electronic Systems, vol. 51, no. 4, pp. 2669-2679, Oct. 2015. doi: 10.1109/TAES.2015.130621

Author Biography

Muhammad Rizwan Mughal



Muhammad Rizwan Mughal was born in Chakwal, Pakistan in 1985. He received his B.E degree in Electrical Engineering, with honors, from the University of Engineering and Technology (UET), Taxila, Pakistan, in October 2007. He received his Ph.D. in the Electronics and Communication Engineering from Department of Electronics and Telecommunications, Politecnico di Torino, Torino, Italy in March 2014.

Since June 2014, he has been an Assistant Professor with the department of Electrical Engineering, Institute of Space Technology, Islamabad, Pakistan. Since July 2018, he has also been associated with department of Electronics and Nano-engineering, Aalto University, Espoo Finland working on innovative design approaches for small satellites. His main interests include plug-and-play design of low-cost small satellites, smart communication solutions for small satellites, wireless solutions for intra-satellite data communication, and testing methodologies for small satellites.

Hassan Ali



Hassan Ali was born in Fort Abbas, Pakistan, in 1996. He received his B.S degree in Space Science, from the Institute of Space Technology, Islamabad, Pakistan, in 2018. The emphasis of his work was on space systems design and remote sensing using

small satellites. His main interests include low cost and smart attitude determination and control systems for small satellites, space mission design and analysis, and interdisciplinary studies.

Anwar Ali



Anwar Ali was born in Mardan, Pakistan, in 1981. He received his B.E. degree in electronics engineering from the NED University of Engineering and Technology (UET), Karachi, Pakistan, in 2004. He received the M.S. degree in electronics engineering and the Ph.D. degree in electronics and communication engineering from Politecnico Di Torino, Italy, in 2014.

He is currently associated with School of Information Science and Technology, Zhejiang Sci-Tech University, Hangzhou 310018, China. His research interests include design and development of power management subsystems of small satellites, attitude sensors and control subsystems of small satellites, thermal analysis and thermal modeling of small satellites, and renewable energy.

Jaan Praks



Jaan Praks (S'98–M'02) received M.Sc. degree in physics from the University of Tartu, Tartu, Estonia, in 1996 and the D.Sc.(Tech.) degree from Aalto University, Espoo, Finland, in 2012. He is currently an Assistant Professor with Aalto University, where he is working on remote sensing instrumentation and nanosatellites with his Microwave Remote Sensing and Space Technology Group. His research interests include microwave remote sensing and space technology.

During his career he has participated in numerous remote sensing projects and measurement campaigns, instrument developments and led the development of Aalto-1 and Aalto-2 nanosatellites. Currently he is leading Satellite Platforms team in Finnish Centre of Excellence in Research of Sustainable Space, where his group is responsible for development of Foresail-1 and Foresail-2 nanosatellite platforms. His research group has spun-off many Finnish New Space companies who build Earth Observation satellite systems in Finland.

Leonardo M. Reyneri



Professor of Electronics at the Polytechnic of Turin, he received M.Sc. cum laude at the Polytechnic of Turin in 1984 and the Ph.D. in 1992.

Prof. Reyneri is currently active in the design of low-cost space systems and modular micro and mini satellites for surveillance and environmental monitoring. He is responsible for a group that brings together academic and industrial partners, with the aim of developing innovative techniques and circuits for low cost modular space systems.

Prof. Reyneri is one of the developers of ARAMIS architecture, which led to the development of innovative technologies, circuit techniques, SW approaches and test methods for low-cost micro and mini-satellites.

Some demos of these innovative technologies will soon be launched in orbit and other demos will fly to the International Space Station (ISS).

Prof. Reyneri has published over 240 articles and holds 8 patents. He has also been a guest editor and referee of international journals and conferences and has worked on program committees or international conference management.

He also spent some periods at the European Space Agency (3 years) and at the University of Pisa (3 years), Edinburgh and Granada. He has been the coordinator of several national research programs, two European projects, together with two major regional projects for the development of innovative ideas.

He is currently cooperating with MIT in Boston (USA), SUPSI in Lugano (CH) and other European universities in the field of nano and microsatellites.